frontiers | Frontiers in Marine Science

TYPE Original Research
PUBLISHED 26 July 2023
DOI 10.3389/fmars.2023.1208052

OPEN ACCESS

EDITED BY
Zhiyu Liu,
Xiamen University, China

REVIEWED BY
Chunxue Yang,
National Research Council (CNR), Italy
Yuanlong Li,
Chinese Academy of Sciences (CAS), China

*CORRESPONDENCE
René Gabriel Navarro-Labastida
RENEGABRIEL.NAVARROLABASTIDA@phd.units.it

†These authors have contributed equally to this work and share first authorship

RECEIVED 18 April 2023
ACCEPTED 05 July 2023
PUBLISHED 26 July 2023

CITATION
Navarro-Labastida RG and Farneti R (2023) The role of shallow and deep circulations in the Tropical Pacific Ocean heat budget. *Front. Mar. Sci.* 10:1208052. doi: 10.3389/fmars.2023.1208052

The role of shallow and deep circulations in the Tropical Pacific Ocean heat budget

René Gabriel Navarro-Labastida[1,2*†] and Riccardo Farneti[2†]

[1]ESFM Doctorate School, Università degli Studi di Trieste, Trieste, Italy, [2]Earth System Physics Section, Abdus Salam International Centre for Theoretical Physics, Trieste, Italy

The Tropical Pacific Ocean plays an important role in setting the global ocean heat content and redistribution. We examined the role of the shallow and deep circulations in the tropical Pacific in unperturbed and transient climate change conditions in a global ocean model. We found that, in the Control state, the shallow circulation is by far the largest contributor to the overall balance of the column, where the balance is set as the residual between advective cooling and warming by vertical diffusive mixing. Subject to surface flux perturbations, changes in the tropical Pacific ocean heat budget can be explained by shallow wind-driven overturning circulation changes. For wind stress anomalies, the shallow ocean heat budget imbalance is directly related to overturning circulation changes, whereas under heat flux perturbations, warming of the shallow ocean is related to strengthened mid-latitude subduction and weakened dense water production at higher latitudes.

KEYWORDS

Tropical Pacific Ocean heat budget, shallow wind-driven overturning cells, surface flux perturbations, super-residual advection, ocean heat content changes

1 Introduction

In addition to the great capacity for storage, distribution, and release of heat, the Pacific Ocean could play a leading role in setting heat content changes under different climate conditions (England et al., 2014; Garuba and Klinger, 2016; Gastineau et al., 2019). However, the role of the shallow overturning has been largely neglected, since global heat content and redistribution are more often associated with the degree of weakening or strengthening of the deep branches of the MOC (Gregory, 2000; Banks and Gregory, 2006; Xie and Vallis, 2011; Marshall et al., 2014; Garuba and Klinger, 2016).

In the tropical oceans, the subtropical cells, or shallow wind-driven overturning circulation, account for most of the heat transport associated with the global Meridional Overturning Circulation (MOC) (Talley, 2003). Moreover, the shallow wind-driven overturning circulation is the primary circulation component in the Pacific Ocean. The circulation is mainly confined within the thermocline, connected with the anticyclonic subtropical gyre and largely driven by easterly wind stress (McCreary and Lu, 1994; Farneti et al., 2014; Song et al., 2018; Graffino et al., 2019).

Here, warm waters are advected poleward by the surface Ekman transport and Western Boundary Current (WBC), cooling and returning equatorward within the subducted layers above the thermocline and eventually upwelling along the equator (McCreary and Lu, 1994; Klinger and Marotzke, 2000; Talley, 2003; McPhaden and Zhang, 2004; Zhang and McPhaden, 2006) (Figure 1A). Water parcels on shallow isopycnals outcrop within the subtropical gyre, interacting with the atmosphere as they flow around the gyre. In contrast, water at deeper isopycnals outcrops within the subpolar gyre, without a direct isopycnic path to the subtropical gyre, being considered unventilated (Figure 1B). The shallow overturning circulation is responsible for a considerable amount of mass and heat transport, particularly in the Pacific Ocean where it is strongest and a deep MOC is absent (Talley, 2003; Garuba and Klinger, 2016).

Under control climate, heat convergence in most of the ocean interior is explained in terms of downward fluxes from large-scale advection and upward fluxes due to mesoscale eddy advection. The joint effect of these processes, often called residual advection, is mostly achieved between the Southern (~60%) and Northern Oceans (~30%), while the remaining contribution is accounted for by the upper tropical oceans as an upwelling–diffusive balance (Gregory, 2000; Exarchou et al., 2014; Exarchou et al., 2014; Kuhlbrodt et al., 2015; Dias et al., 2020).

Isopycnal mixing is an additional mechanism affecting the global heat balance, and is particularly important in the Southern Ocean and the subtropics, where most water mass convergence and associated heat transport are achieved along sloping isopycnals (Gregory, 2000). These major drivers of the overall heat budget can be combined into one single advective term, the superresidual

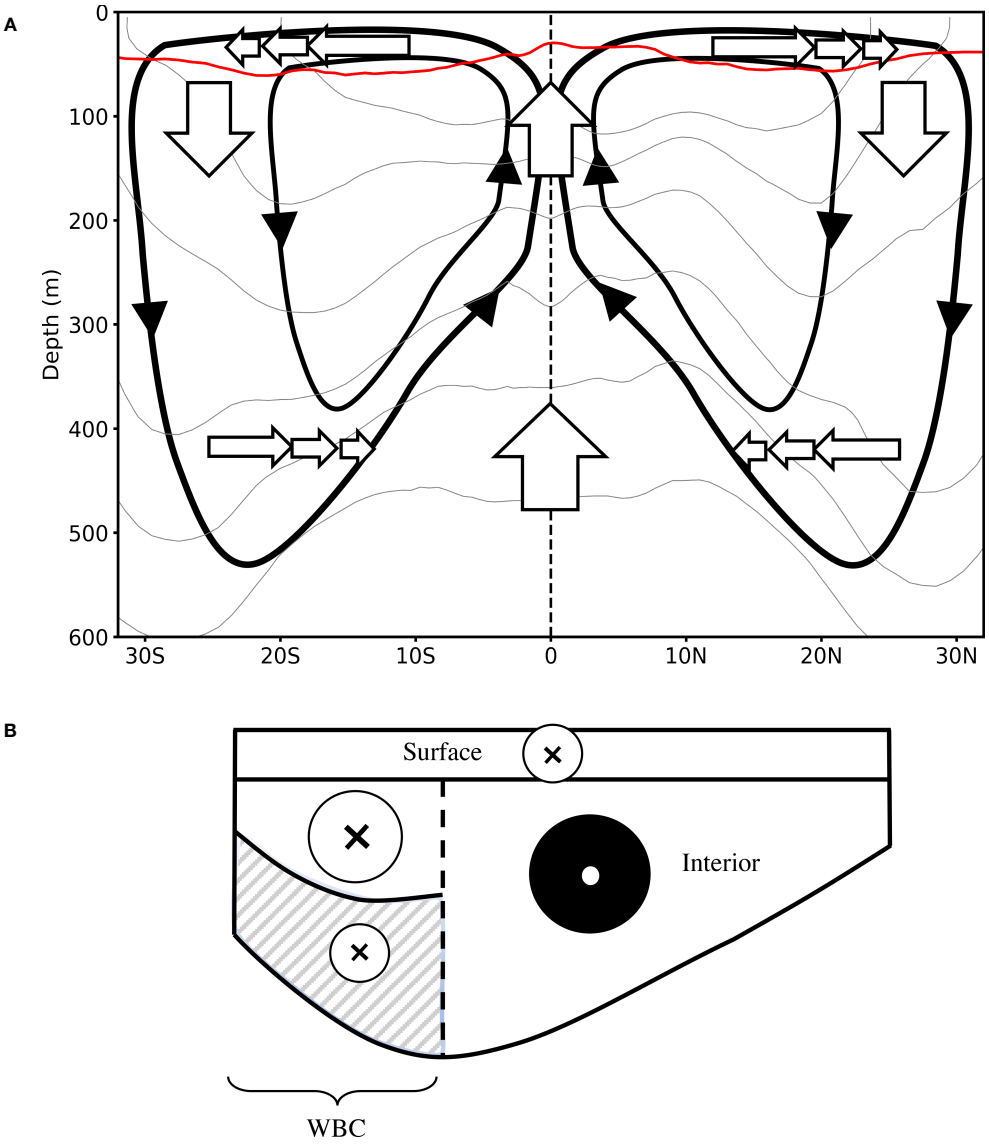

FIGURE 1
(A) Time-mean and zonally integrated Pacific Ocean shallow MOC. The isopycnal field (gray contours) and mean mixed layer depth (red line) are also shown. White arrows depict the main circulation branches. **(B)** Schematic zonal section of the shallow MOC across 24°N, including surface, WBC, and interior transports. Balance excludes deeper levels of the WBC (shaded area).

advection (Kuhlbrodt et al., 2015; Dias et al., 2020). Using the superresidual advection framework, Dias et al. (2020) divided the global ocean heat budget into two opposite regimes: the upper and the interior ocean. The upper ocean regime dominates poleward of 35° and explains most of the residual advection global balance. In contrast, the interior regime is mainly located at low latitudes as an upwelling–diffusive balance. The connection between both regimes is achieved by redistribution of upper mixed layer waters along isopycnal surfaces and mixing of this water with adjacent water masses in the interior ocean (Dias et al., 2020).

Although these regimes are often studied in the context of ocean heat uptake (Gregory, 2000; Exarchou et al., 2014; Kuhlbrodt et al., 2015), understanding of the mechanisms that lead to ocean heat uptake during climate change requires a detailed understanding of the ocean heat balance (Exarchou et al., 2014; Dias et al., 2020). Moreover, a full understanding of the ocean's heat balance relies not only on the description of the different components of the budget but also on the different dynamical mechanisms involved. Here, we present a quantitative analysis of the role of each physical process in setting the heat budget and transport of the tropical Pacific under control and climate change surface forcing anomalies. In our framework, the Tropical Pacific is divided into vertically dependent regimes based mainly on dominant dynamical processes. Our procedure is based on a definition of the different vertical regimes encompassing not only thermohaline characteristics and distribution of water masses, but also the main large-scale ocean dynamical features. Thus, our analysis provides an assessment of the separate contribution of the shallow overturn from the unventilated and remotely forced deep ocean to the Tropical Pacific heat budget.

In *Section 2*, we describe the model used and our experimental setup. Details about the heat budgets calculation (*Section 2.2*) and the meridional transports of mass and heat (*Section 2.3*) are also provided. In *Section 3*, the main results are presented and discussed. *Section 4* summarizes our findings.

2 Materials and methods

2.1 Description of the ocean model and experimental design

In this study, we used the ocean general circulation model NOAA-GFDL Modular Ocean Model version 5 (MOM5) (Griffies, 2012; Todd et al., 2020). MOM5 is a free-surface primitive equation model and uses the $z\star$ -vertical coordinate. The horizontal resolution is 1° with refined meridional resolution equatorward of 30°. It uses 50 vertical levels, with 10 levels in the top hundred meters. Subgrid mesoscale processes are parameterized with the Gent-McWilliams skew-flux closure scheme (Gent and McWilliams, 1990; Gent et al., 1995; Griffies, 1998) and submesoscale eddy fluxes according to Fox-Kemper et al. (2008) and Fox-Kemper et al. (2011). Vertical mixing is represented with a K-profile parameterization (Large et al., 1994).

For our experiments, we followed the protocol proposed by the ocean-only Flux-Anomaly-Forced Model Intercomparison Project (FAFMIP; Todd et al., 2020) in order to exclude any coupled feedback. A spin-up was performed by integrating the model towards a near-equilibrium state, using as forcing fields the total mass flux of liquid precipitation plus liquid runoff minus evaporation, net heat flux, and surface wind stress (see Todd et al., 2020). An ensemble of pi-Control CMIP5 AOGCMs was used to generate climatologies for all fluxes. Restoring of both sea surface temperature (SST) and sea surface salinity (SSS) employs a time scale of 2 and 3 months, respectively (Todd et al., 2020).

After equilibrium, a restored Control simulation was obtained through an additional 70 years of integration. During this Control, total effective air–sea heat and freshwater fluxes were stored at daily intervals, including restoring-induced SSS fluxes. Finally, a twin second Control was obtained with SSS restoration deactivated and by prescribing the effective heat and freshwater fluxes diagnosed from the first Control. Differences between both controls have been quantified and are negligible. The flux-forced Control is used as the reference state, and will henceforth referred to as the Control simulation.

Sensitivity experiments are forced by FAFMIP surface flux perturbations, derived from a set of 13 CMIP5 AOGCMs, where each surface flux represents the transient response of the climate system to a doubled CO_2 concentration under the idealized scenario 1pctC02 (Gregory et al., 2016). Anomalous fields are computed as the difference between the climatological monthly time-means of years 61–80 of 1pctCO_2 and the corresponding time-means of the non-evolving and unforced variability equilibrium state known as pre-Industrial or piControl run (Taylor et al., 2011). All experiments are global, 70 years long, branching off from the Control simulation and forced by the Control effective surface fluxes plus the FAFMIP momentum (faf-stress) or heat (faf-heat) anomalous fluxes (Figures 2, 3). In faf-stress, global zonal and meridional wind stress perturbations are added to the momentum balance equation, whereas faf-heat adds heat flux perturbations to the total surface downward heat flux.

The Tropical Pacific Ocean is vertically divided into depth-dependent integrals representative of shallow and deep circulations. The shallow ocean, involving the subtropical overturning cells, spans in both hemispheres from the tropics up to the mid-latitudes where subduction of surface water takes place (McPhaden and Zhang, 2004), approximately 32° in our model. In the vertical, it is bounded at the top by the mixed layer and at the bottom by the deep ocean. In the latitudinal extent, the shallow ocean extend from near the Equator up to the latitude of minimum zonal wind stress (32°N and 30°S, respectively). Here, mixed layer depth estimation consists of the determination of the vertical level at which temperature change from the surface is equal to 0.5°C, as suggested by Levitus (1982). Our definition for the shallow overturn considers all vertical levels away from the influence of both the surface mixed layer and the deep ocean circulation.

Our definition of the Shallow Wind-driven Overturning Circulation differs from that of subtropical cells (STCs) by previous studies (McCreary and Lu, 1994; McPhaden and Zhang, 2002; Zhang and McPhaden, 2006; Farneti et al., 2014; Graffino et al., 2018). Traditionally, the STC is characterized in terms of equatorward mass transport within the upper thermocline. In

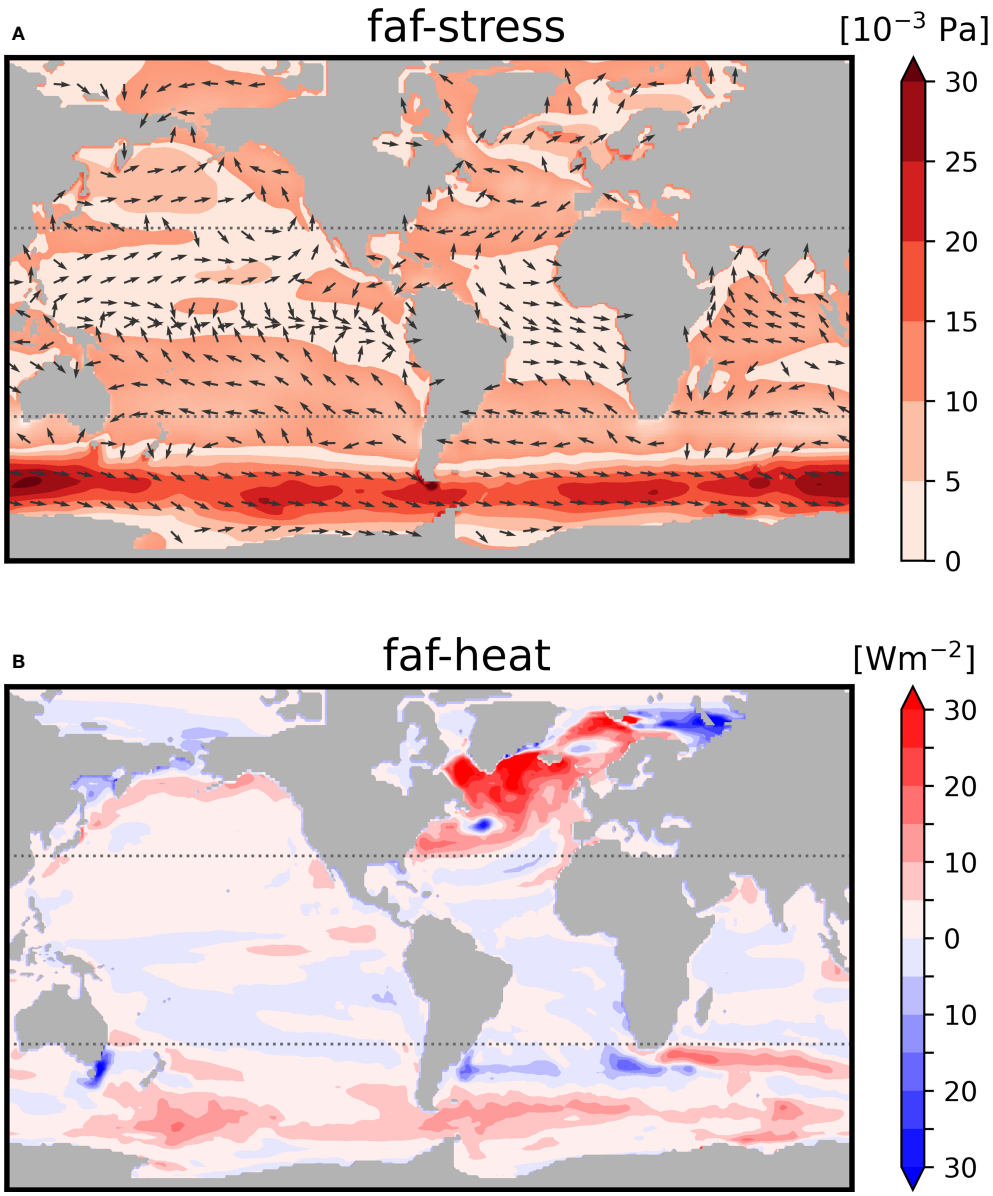

FIGURE 2
Annual mean surface flux perturbations from FAFMIP. In **(A)**, arrows indicate the direction of the surface momentum flux perturbation in faf-stress. In **(B)**, heat flux perturbations for faf-heat are defined as positive downward, with positive values representing warming of the ocean. The Tropical Ocean considered in this study is bounded between 30°S and 30°N (dotted lines).

contrast, our definition encompasses a wider latitudinal extent and includes not only the subtropical overturning cells but also the lower-latitude tropical overturn and equatorial upwelling region, and intentionally avoids the mixed layer region.

In the case of the deep ocean, this region is defined as the region below the deepest vertical limit of the shallow overturn (Figure 1A). As suggested by Talley (2003), we defined the base of the shallow overturn as the maximum subducting level at the subtropical gyre. The definition implies using meridional zonally integrated Sverdrup circulation sections and determining either the vertical level at which the transport is nearly zero or simply by determination of the deepest closed streamline. Once the mixed layer depth and the base of the overturn are determined, the separate contribution from the shallow circulation can be estimated, minimizing the influence of both atmosphere and the deep ocean.

Explicitly, the deep ocean encompasses all the vertical levels of the ocean below the shallow overturn up to near the bottom of the ocean. Given the minimization of the mixed layer influence and the determination of the shallow ocean, all the remaining circulation contributions must represent the circulation related to the deep branches of the MOC. However, the above-mentioned partitioning of the water column is only for the purpose of the determination of the budget integrals. In *Section 2.3*, we will provide a link between the heat budget analysis and an independent analysis of the dominant circulation patterns in the water column.

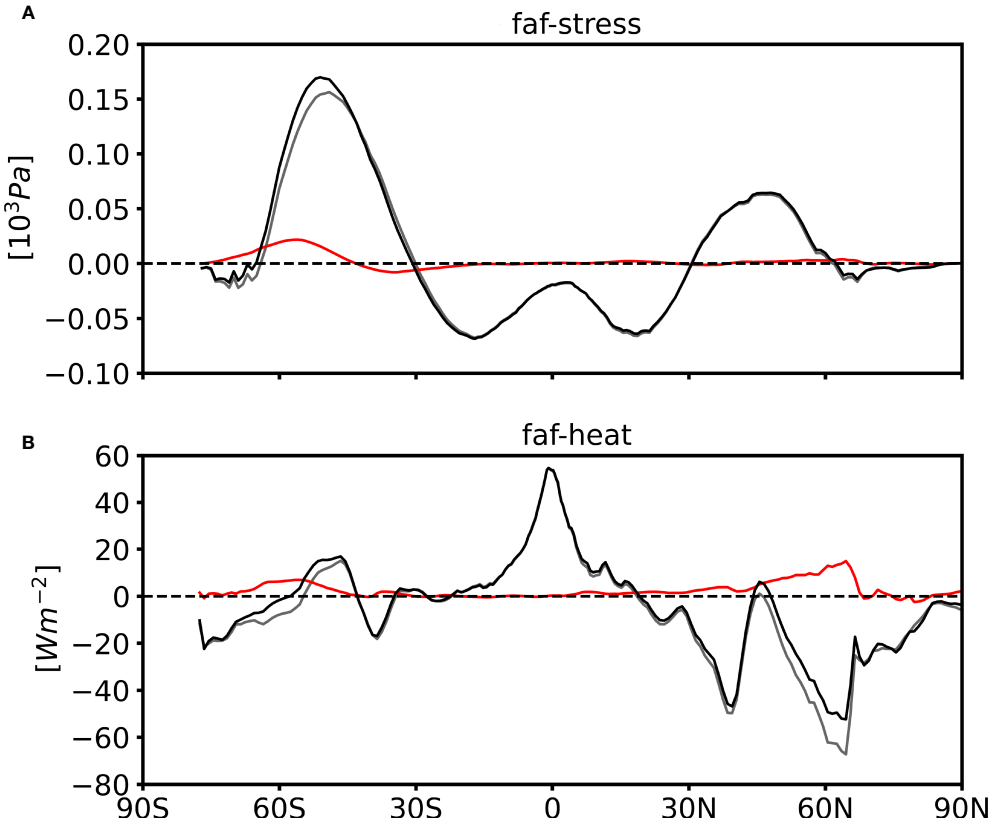

FIGURE 3
Zonal and annual mean surface flux perturbations from FAFMIP. Zonally averaged surface wind stress in faf-stress **(A)** and surface heat flux in faf-heat **(B)**. The equilibrium state, perturbations, and their joint effect are shown in gray, red, and black, respectively.

2.2 Ocean heat budget calculation

The following provides a diagnostic accounting of the ocean heat budget for a grid cell in the model. The relative contribution of each physical process to the overall heat budget, concerning the equilibrium state and perturbed climate conditions, is quantified using the three-dimensional process-based tendency diagnostics for prognostic temperature (Griffies et al., 2016; Dias et al., 2020). Such a procedure allows us to determine in physical terms the processes responsible of setting the overall heat storage balance.

The time tendency for the heat content in a grid cell per unit horizontal area, expressed as a semi-discrete finite volume formulation within the grid cell, is shown by Griffies et al. (2016)

$$C_p\,\rho_0\,\frac{\partial\,(T\,\mathrm{d}z)}{\partial\,t} = Q - \nabla\cdot[\rho_0\,\mathrm{d}z(\boldsymbol{u}\,T + \mathbf{F})] \qquad (1)$$

where T represents the temperature of a grid cell, C_p is the heat capacity coefficient, and $\rho_0\,\mathrm{d}z$ is the mass of seawater per horizontal area in a grid cell with ρ_0 being the reference density and d $z$being the grid cell thickness. The tracer fluxes at the surface of the ocean are represented as Q. Generalized three-dimensional velocity is expressed as $\boldsymbol{u}$ while $\boldsymbol{F}$ accounts for the parameterized subgrid-scale processes, including circulation, diffusion, eddies, and vertical mixing.

The tracer formulation's vertical extent is time-dependent, which implies that each heat budget term scales according to the thickness of the cell. In contrast, the horizontal cross-sectional area is time-independent, which implies area normalization if the tracer grid cell is multiplied by the horizontal area.

The time tendency for the heat content for each grid cell over an ocean column arises as the convergence of advective processes ($\boldsymbol{u}\,T$) in addition to subgrid-scale heat fluxes ($\boldsymbol{F}$) (Eq. 1) and the net time tendency for the heat content is represented as the convergence of the general tracer flux F_{xz} and is expressed as

$$\partial_t\,T_{\mathrm{net}} = F_{xz} = \partial_t\,T_{\mathrm{adv}} + \partial_t\,T_{\mathrm{eddy}} + \partial_t\,T_{\mathrm{iso}} + \partial_t\,T_{\mathrm{dia}} + \partial_t\,T_{\mathrm{swh}} \qquad (2)$$

Here, $\partial_t\,T_{\mathrm{net}}$ represents the model diagnosed tracer for the time tendency in a grid cell, and is equivalent to the temperature time derivative in the advective–diffusive equation, or can be expressed in terms of a generalized tracer flux F, which is the convergence of advective or subgrid-scale fluxes crossing grid cell faces. The diagnosed advective processes account for the model prognostic advection ($\partial_t\,T_{\mathrm{adv}}$) and parametrized eddy-induced advection ($\partial_t\,T_{\mathrm{eddy}}$), including both mesoscale and submesoscale flux components (Fox-Kemper et al., 2008; Fox-Kemper et al., 2011; Gent and McWilliams, 1990). Within the diagnosed diffusive mixing processes, we distinguish among isopycnal ($\partial_t\,T_{\mathrm{iso}}$) and diapycnal mixing ($\partial_t\,T_{\mathrm{dia}}$). The first refers to diffusion oriented

along neutral or isopycnal surfaces and the second encompasses vertical convection and vertical diffusion, including parameterization of diapycnal diffusion due to tidal mixing, shear instabilities, double diffusion, mixing due to convective instabilities, and the overflow parameterization of dense water flowing down topographic slopes.

Since our formulation does not take into account mixed layer depths, contributions related to the non-advective radiative transfer are neglected (i.e., $Q = 0$). In contrast, we included a diagnostic related to parameterized oceanic absorption of downward solar radiation ($\partial_t T_{\mathrm{swh}}$). This term stands for shortwave heat flux at the bottom of a tracer grid cell face, generally expressed as the attenuated downwelling shortwave radiative heat per unit area incident at the ocean surface. Owing to the similar nature of both contributions, diapycnal mix and shortwave heat penetration terms are grouped together and presented as a vertical diffusive processes term (vDIFF). The expression $\partial_t T_{\mathrm{net}}$ stands for both the iterated model diagnosed term and the linear sum of all the different components. By construction, temperature tendency diagnostics should close the heat budget. However, both estimations are not necessarily equivalent implying a heat budget residual.

Imbalances can be explained in terms of two non-quantified contributions, namely, non-diagnosed processes (diffusive mixing) and non-resolved high-frequency variability (i.e., interannual variability). In particular, non-local turbulent vertical flux boundary layer parameterization, overflow schemes, and mixing across unresolved straits are contributors to such imbalance (Griffies et al., 2016). Despite the fact that such components are indeed diagnosed by the model, those quantities are not considered in our analysis, since they have been quantified to be small. In contrast, the component related to the so-called interannual variability is explained in terms of an inaccurate closure budget due to the time scale on which tendencies are saved. All diagnostics used here are saved as annual averages despite the fact that they are diagnosed in the model at each time step. In order to close the budgets, such contribution is added to the vertical diffusive component given the diffusive mixing nature of the non-diagnosed terms.

It is important to note that imbalances do not arise because of model drift. In the equilibrium state, the global mean net tendency is near-zero but not exactly zero, a common feature among global climate models due to the typically longer time scales required for the deep ocean to reach equilibrium (Exarchou et al., 2014). Such contributions are rather small with no significant impact on the determination of the budgets. In contrast, we refer to imbalances as any transient change (warming or cooling) in the ocean heat content time rate of change (heat storage) derived from the perturbed climate conditions.

Here, we are interested in grouping all of the advective terms together, so that the superresidual advection encompasses the contribution from the parameterized flow, and the super-residual advection (srADV) is defined as

$$\partial_t T_{\mathrm{srADV}} = \partial_t T_{\mathrm{adv}} + \partial_t T_{\mathrm{eddy}} + \partial_t T_{\mathrm{iso}} \quad (3)$$

Lastly, previous studies have adopted weighting functions in the time domain to assess changes between the first and last decade of the experimental period (Gregory et al., 2016; Todd et al., 2020). In our study, we are interested in the transient response of the ocean and none of the results make use of any type of weighting and the transient response of each heat budget is evaluated relative to the equilibrium state solution.

2.3 Meridional mass and heat transport calculation

The Pacific Ocean shallow wind-driven overturning circulation is described in terms of the meridional mass transport. Our estimations consider mass balance adjusted to zero across 24°S and 24°N. As in Talley (2003), the selection of such latitudes is based on the detection of three circulation features: a strong overturning circulation (i.e., surface poleward and subsurface equatorward transports), a well-defined poleward WBC flow, and a mid-latitude subducting area. In addition, the selected latitude is meant to minimize the effects of water recirculation by the tropical subsurface overturn (between 5° and 10° latitudes).

Our results refer to the annually averaged meridional transport under both sensitivity cases and the equilibrium-state solution, with time-averaged spanning over the last decade of the simulation period. The zonally integrated transport for different density classes is also included. Each water mass is classified according to its ventilation level on the basis of climatological annual means (see Table 1). Procedure implies partitioning the water column in terms of the isopycnal distribution and their level of outcropping. The density limits between the different water masses are determined as the outcropping density level at the given latitude when possible, or simply based on the density field distribution.

As suggested by Talley (2003), four types of water classes are defined: upper, intermediate, deep, and bottom waters. The upper waters refer to low latitudes waters bounded by the outcropping isopycnal at 30°S–30°N. Despite the motion of this layer being arguably primarily wind-driven, we did not explicitly isolate such contribution, so transport inside this layer includes both Ekman poleward transport and the geostrophic transport related to the gyre circulation. The intermediate waters refer to mid-latitude waters bounded by outcropping isopycnal surfaces between the region 30° and 60°. The deep water is immediately located below the intermediate water and is only ventilated through the Southern Ocean. Bottom waters are located in the densest layers.

The overall volume transport is adjusted to zero mass balance, which means compensation of volume between layers. We did not estimate any water mass conversion rates, and our calculations are simply based on the assumption of effective subduction rates. The northward Ekman transport is zero at approximately 30°N and all northward Ekman transport at 24°N is at a much lower density than the maximum subducted density; hence, we assumed that all Ekman flow at 24°N loses buoyancy and joins the southward geostrophic flow of the subtropical gyre.

TABLE 1 Density intervals [kg m^{-3}] for each water mass in both Northern Hemisphere (NH) and Southern Hemisphere (SH).

	Lat	NH	SH
Upper 1	24° N,S	1,031.87	1,032.11
Upper 2	30° N,S	1,032.80	1,032.73
Upper 3	40° N,S	1,033.89	1,033.93
Intermed. 1	45° N,S	1,034.66	1,034.67
Intermed. 2	60° N,S	1,035.04	1,036.28
Intermed. 3	64° N,S	1,035.35	1,036.57
Deep 1	70° -,S	1,036.20	1,036.73
Deep 2	–	1,036.80	1,036.80
Deep 3	–	1,036.90	1,036.90

The latitude at which each density level outcrops to the surface is shown (Lat), and if the outcrop occurs in either one or both hemispheres. When an outcrop latitude is not observed, level detection was made *ad hoc* based on the density field characteristics.

Additionally, within the shallow overturning cell, volume transport is divided into the Western Boundary Current (WBC) transport and interior equatorward transport (Figures 1, 4). The outcrop between equatorward interior flow and WBCs is meant to avoid regions of recirculation water masses (McPhaden and Zhang, 2004; Zhang and McPhaden, 2006). All of the Ekman transport is assumed to remain in the subducting subtropical gyre. To balance the returning flow, we arbitrarily use only the lightest and warmest part of the WBC upper layer. Remaining volume transport is assumed to flow outside of the gyre towards the subpolar region and to return as intermediate or deep water.

Heat transport (HT) is calculated from the zonally integrated transports in isopycnal layers. Expression for the lateral heat transport through a vertical cross-sectional area requires velocity and temperature and is expressed as

$$\mathrm{HT} = \int \rho \, c_p (v\,\theta)\, \mathrm{dA}, \tag{4}$$

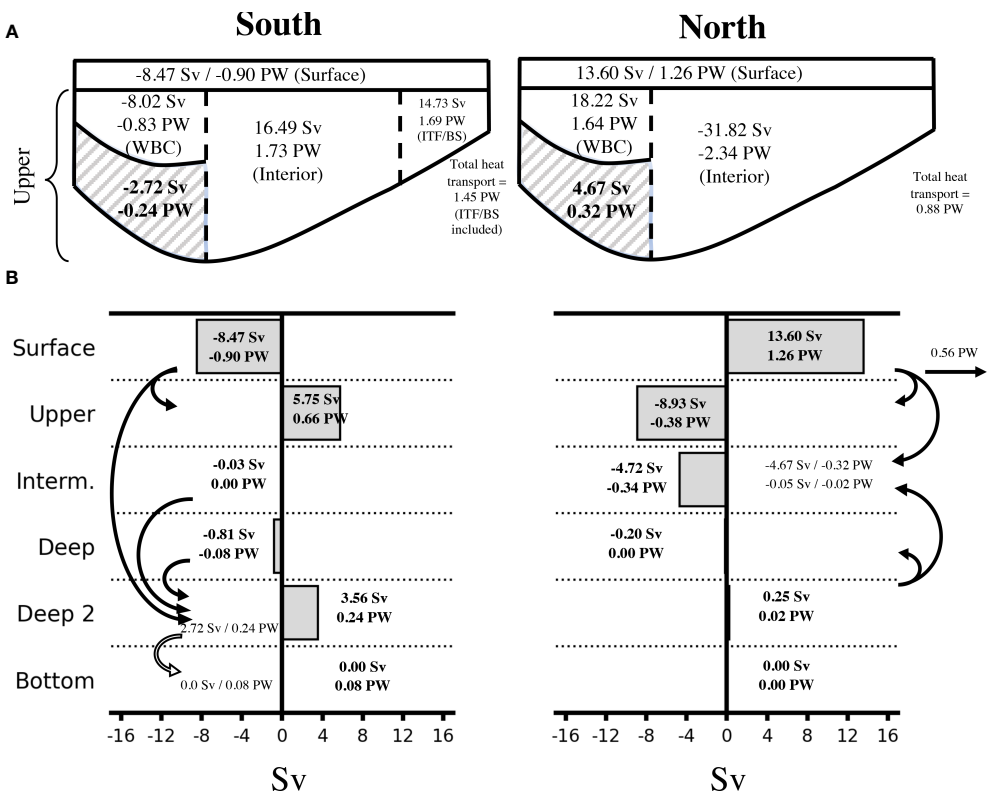

FIGURE 4
Pacific Ocean meridional mass (in Sv) and heat (in PW) transports, in both Southern and Northern Hemispheres, in the control simulation. Computations consider mass balance adjusted to zero across 24°S and 24°N, respectively. **(A)** Shallow Overturning Cell schematics inside the Subtropical Gyre. Meridional transport inside the cell is divided into surface poleward transport, the Western Boundary Current transport (WBC), and the interior equatorward transport. Balance inside the overturning cell excludes transport within deeper levels of the WBC (shaded area), which flows outside of the gyre towards the subpolar region. In the Northern Hemisphere, mass balance in the cell is achieved by subtracting 14.73 Sv. Such contribution is identified as the Indonesian Throughflow and Bering Strait contributions together (ITF/BS). In the Southern Hemisphere, the total heat transport estimation includes the ITF/BS contribution (1.69 PW), while the shallow overturning term is zero by construction. **(B)** Zonally integrated transport for different density classes within each water mass is classified according to its ventilation level. The Upper transport refers to the sum of all fluxes within the Shallow Overturning Cell (poleward WBC plus equatorward interior flow, excluding the surface term). Other terms refer to meridional mass transports below the cell. The curved arrows indicate the mass transfer between water classes and heat transports that go with the mass balances. Mass and heat transports assume that the transfer occurs preferentially between most adjacent layers. Arrows are shown for both the Southern (left) and Northern (right) Hemispheres. Any heat exchange that does not imply mass exchange is indicated as a white arrow.

where ρ, v, C_p, and θ are the density, velocity normal to the area, the specific heat of seawater, and potential temperature, respectively.

3 Results

3.1 Tropical Pacific Ocean heat budgets

The volume-integrated heat budgets for the Northern Hemisphere (NH) and the Southern Hemisphere (SH) Tropical Pacific Ocean are shown in Figure 5, with vertical integrations accounting for the total column, the Shallow Wind-driven Overturn, and the deep ocean (mixed layer depths not included). In the Control simulation (Figures 5A, B) the tropical Pacific Ocean heat tendency imbalance is near-zero but not exactly zero (NET), a common feature in global climate models due to the very long time scales required for the deep ocean to reach equilibrium (Exarchou et al., 2014).

In general, heat balance arises as the compensation between vertical diffusive warming (vDIFF) and the residual advection due to resolved (ADV) and parameterized eddy processes (EDDY), along with eddy mixing terms (ISO). As in Kuhlbrodt et al. (2015) and Dias et al. (2020), here we will refer to super-residual advection (srADV) as the sum of the advective terms and eddy mixing terms. In fact, the net balance can be simplified as a compensation between super-residual advection (srADV) cooling and vertical diffusive warming (vDIFF). The use of the super-residual advection framework allows us to simplify the description of the heat balance analysis. All the individual contributions to the heat balance (ADV, EDDY, rADV, and ISO) are presented in Figure 5, but heat budget changes will be discussed only in terms of the super-residual advection framework (srADV and vDIFF).

The observed balance seems to disagree with the two opposite vertical regimes proposed by Dias et al. (2020), but it arises from excluding the influence from the mixed layer. Here, both regimes are included in the ocean interior defined by Dias et al. (2020). Our results are thus in accordance with the ocean interior regime proposed by Dias et al. (2020) but also suggest that most of the balance is achieved within the shallow wind-driven overturn. This is confirmed by the zonally integrated heat budget within the ocean column (Figures 6A–C), which shows a balance between downward warming by a vDIFF flux and upward cooling by a srADV flux. The balance holds over the whole column, but it is particularly intense within the upper levels of the shallow ocean, near the mixed layer, and within the subducting areas, suggesting a strong association with the convergence and subduction of surface tropical waters. This is in accordance with the circulation pattern held by the cell, which promotes the removal of upper ocean water towards the interior ocean (Dias et al., 2020).

According to our definition and partitioning of the water column, although we have excluded the surface processes, the warming of the rest of the column comes from the mixed layer. Transfer of heat comes from the mixed layer heat transfer from the mixed layer toward the interior ocean given the circulation pattern held by the cell. The last is by removing mixed layer water toward deeper levels, mainly along the isopycnal field toward the interior ocean (Dias et al., 2020). The last is actually in accordance with vDIFF warming and srADV cooling taking place mainly in the subducting area (30°N and 30°S) (see Figures 6B, C).

In faf-stress, net imbalance is the result of an intensification of the srADV cooling compensated by vDIFF warming in both hemispheres (Figures 5C, D). In the NH, the negative imbalance is given by the srADV in the shallow ocean, but in the SH, the positive imbalance is produced by enhanced vDIFF in the deep ocean. In contrast, in faf-heat, total warming imbalances are set primarily by strengthened vDIFF (Figures 5E, F). In both hemispheres, the source of heating is the strengthened vDIFF warming and reduced srADV cooling. However, while the shallow ocean in the NH holds nearly 70% of the total net warming imbalance, it only accounts for approximately 10% in the SH (Table 2).

According to the volume-integrated budgets, in faf-stress, net imbalance is the result of intensified srADV and vDIFF balance, whereas in faf-heat, warming in both hemispheres is set by strengthened vDIFF and weakened srADV mainly in the deep ocean.

Both in faf-stress and faf-heat, imbalances are located nearly at the same vertical level and, given the different vertical penetration of the cell in the two hemispheres, the imbalance is promoted by the shallow overturn in the NH and the bottom circulation in the SH (Figures 6D–I). This reasserts the importance of separating the ocean into dynamical regimes, rather than using vertical budget integrations based solely on arbitrary selection of boundaries between layers. Our results highlight a local redistribution of heat from the surface to the deep ocean, since imbalances in the unventilated tropical Pacific appear to be linked to subtropical surface anomalies, advected to the deep ocean along mean isopycnal pathways.

3.2 Shallow and deep meridional transports

Because ocean heat transport is linked to water mass transformation, it is useful to estimate the relative contribution of the different water masses in the overall heat transport (Talley, 2003). Meridional transports are computed for the shallow wind-driven overturning cells and the zonally integrated transport at different density classes, with each water mass classified according to its ventilation level. Heat budget calculation is presented for each experiment. The meridional transport inside the cell is divided into surface poleward transport, WBC contribution, and the interior equatorward transport, computed both at 24°S and 24°N. Balance inside the overturning cell excludes transports within deeper levels of the WBC, which flows outside of the gyre towards the subpolar region (Talley, 2003). Estimations consider mass balance adjusted to zero, but there is a positive net heat transport for this mass-balanced shallow overturn (Tables 3, 4).

The zonally integrated mass and heat transport within different water masses is shown in Figure 4 for the Control. In this case, the transport associated with the upper layer represents the residual between the total poleward WBC flow and the equatorward interior

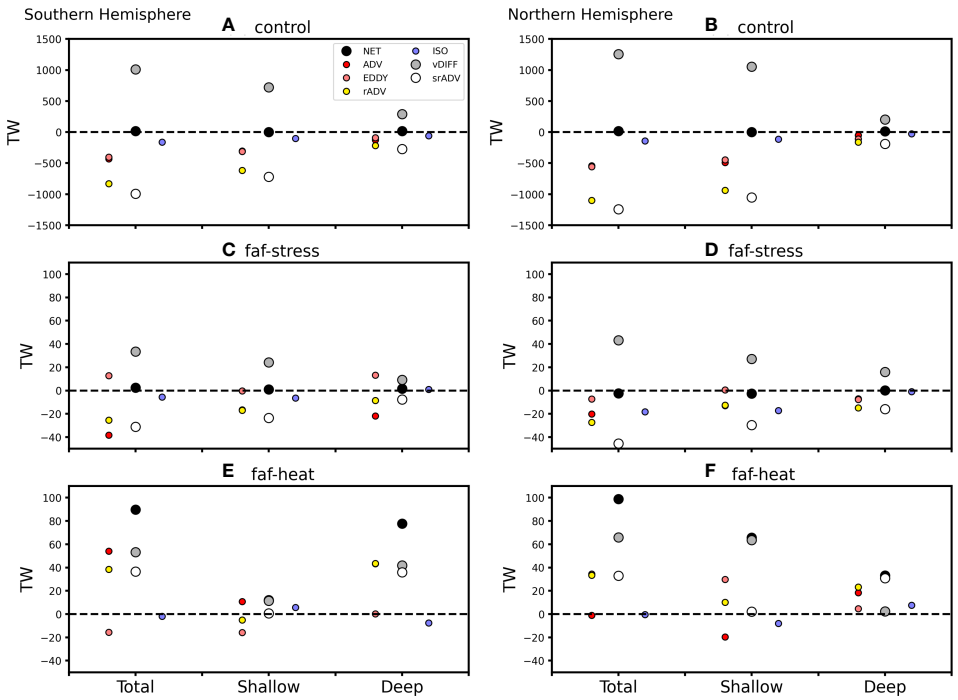

FIGURE 5
Volume-integrated heat budgets for the Southern (left) and Northern (right) Tropical Pacific Ocean. Vertical integrations account for the Total, Shallow, and Deep ocean (mixed layer not included) for the control simulation **(A, B)**, faf-stress **(C, D)**, and faf-heat **(E, F)**. Budget components (in TW $\equiv 10^{12}$ J s^{-1}) are the net heat storage (NET), model prognostic advection (ADV), parameterized eddy-induced advection (EDDY), the residual mean advection (AVD+EDDY, rADV), diffusive isopycnal mix (ISO), vertical diffusive processes (vDIFF), and the super-residual advection term (rADV+ISO, srADV). The terms involved in the simplified heat balance (i.e., super-residual advection framework) are represented with bigger markers. All budgets are time-mean for the last decade. **(C–F)** refer to anomalies with respect to the equilibrium case.

flow. All remaining layers refer to meridional mass transports below the cell. In the Control simulation, in the NH, the shallow overturning cell recirculates nearly 32 Sv and 2.34 PW according to the interior flow (Figure 4A). The net heat transport by the shallow overturning contributes nearly 65% of the total heat transport. Poleward transport by the cell is given not only by the surface Ekman flow but also by the WBC in both hemispheres (~ 60%), a contribution related to the geostrophic circulation within the subtropical gyre.

In contrast, according to the zonally integrated transports, most of the surface northward transport returns within the cell (> 65%), while the rest returns as intermediate water mixed with upwelled deep water. Transfer between water mass classes, assuming the transfer occurs preferentially between most adjacent layers, is schematically represented with vertical arrows in Figure 4B. In fact, in terms of the equatorward intermediate water, this is mostly composed of surface water with a small contribution from upwelled deep water.

In the SH, the shallow overturning cell recirculates nearly 16~Sv and 1.7~PW according to the interior flow. As in the NH, WBC transport is responsible for nearly 50\% of both poleward mass and heat transports. In the zonally-integrated mass and heat transports, the total and shallow overturning transports are fully accounted for by the surface layer. Most of the surface poleward transport returns within the cell as upper waters (~ 70%), while the rest returns as converted deep waters mixed with poleward downwelling intermediate waters, and the contribution associated with intermediate waters is rather secondary (20%). Deep waters promote a diffusive transfer of heat towards the bottom of 0.08 PW, which nearly represents 25% of the heat convergence within deep waters. The shallow ocean determines nearly the entire meridional mass and heat transports in the NH (> 90%) and most of the transports in the case of the SH (~ 70%). Moreover, the WBC plays an important role in the overall poleward shallow overturn transport of both mass and heat (> 50%).

Next, we focus on the response under surface flux perturbations. The relative change of each meridional mass transport component is computed with respect to the equilibrium state and shown in brackets (for details, see Tables 3, 4). In faf-stress, the NH shallow overturning cell reveals an overall weakening (Figure 7A). The weakened signal is explained in terms of a weakened interior equatorward transport (–11%) and WBC transport (–20%). In contrast, the production of dense water by the cell is significantly increased given by the increased surface poleward transport. This is in accordance with the strengthened equatorward intermediate and deep water mass production and also the weakened poleward deep water mass production (–20%). These changes can be explained in terms of reduced mid-latitude subduction, according to the zonally integrated mass and heat transports (Figure 7B). Although faf-stress

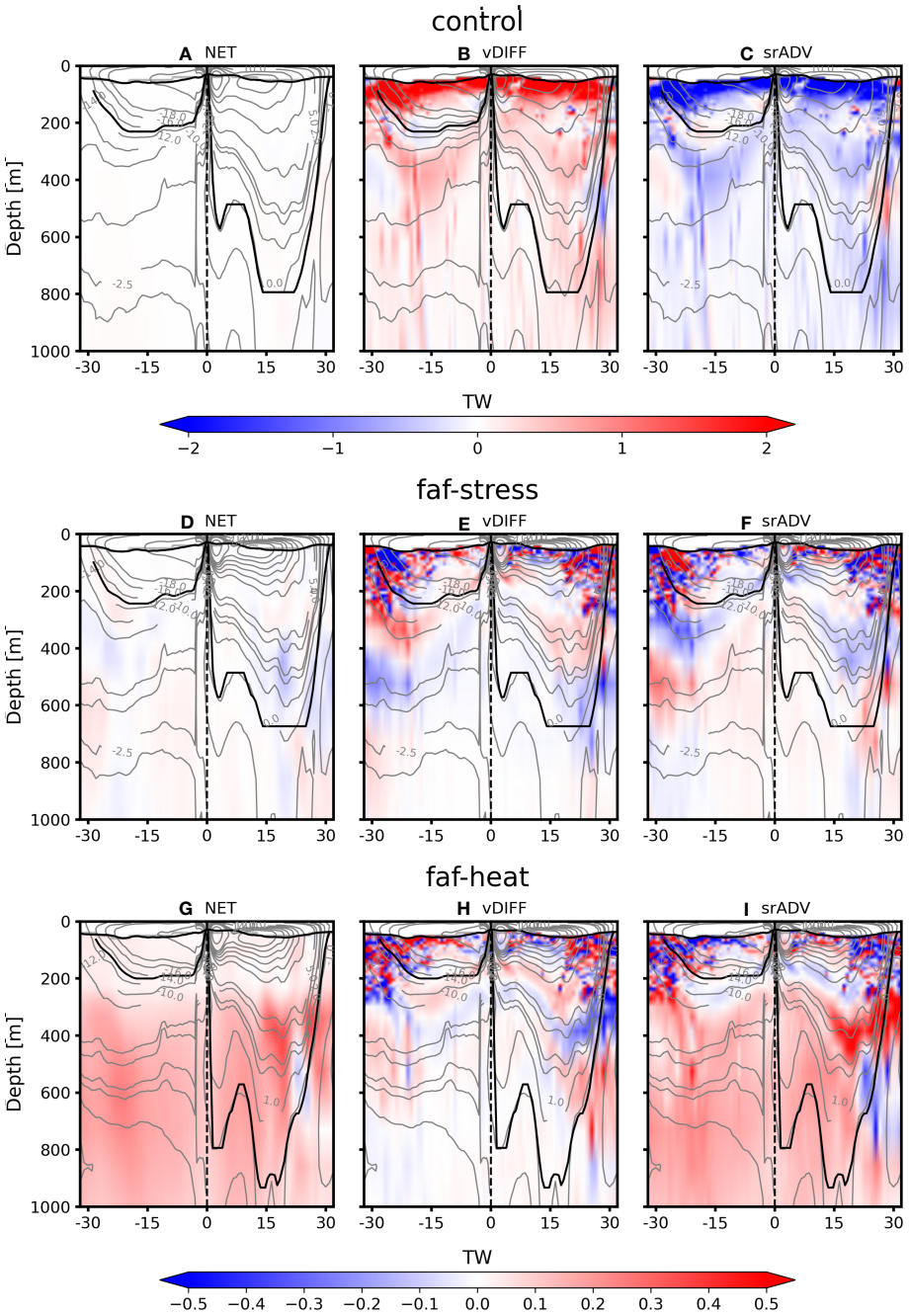

FIGURE 6
Zonally integrated heat budgets for the tropical Pacific Ocean in the control simulation **(A–C)**, faf-stress **(D–F)**, and faf-heat **(G–I)**. The base of the shallow overturn is shown as the thick black line. Meridional transports (in Sv $\equiv 10^9$ kg s^{-1}) are also shown (gray contours). Budget components (in TW $\equiv 10^{12}$ J s^{-1}) are as in Figure 5.

imposes relatively weak reduction in both tropical and subtropical wind stress (Figure 2), these changes are able to promote weakening of the mid-latitude subduction and slowing down of the overturning cell. Moreover, circulation changes are in agreement with observed net heat imbalances observed in both the shallow and deep ocean, by increased srADV cooling and vDIFF warming. While strengthened circulation produces cooling of the shallow ocean, intensified intermediate water production produces warming of the deep ocean (Figure 8A).

The SH shallow overturning cell shows an overall strengthening. This is based on the strengthened surface mass and heat transport and the strengthened interior equatorward transport. This is in line with the observed strengthening wind stress over the SH Pacific Ocean (see Figure 2A). However, intensification of the overturn seems to reduce the poleward transport outside of the cell, inhibiting the formation of dense water. Moreover, given the increased mid-latitude subduction of surface water by the cell, the production of dense water is reduced,

TABLE 2 Volume-integrated heat budgets for the Tropical Pacific Ocean (mixed layer not included) in each experiment.

	NET	ADV	EDDY	ISO	DIA	SWH	Unres	rADV	srADV	vDIFF
Control										
Northern Hemisphere										
Shallow	1.3	−490.9	−447.9	−114.6	−65.9	1005.5	115.2	−938.8	−1053.4	1054.7
Deep	13.2	−50.2	−110.1	−28.9	67.3	119.7	15.4	−160.3	−189.2	202.4
Total	14.5	−541.1	−558.0	−143.5	1.4	1125.1	130.6	−1099.2	−1242.6	1257.1
Southern Hemisphere										
Shallow	0.3	−304.0	−312.6	−102.5	−171.9	810.0	81.3	−616.6	−719.1	719.4
Deep	15.9	−126.7	−88.8	−57.4	173.3	103.1	12.3	−215.5	−272.8	288.7
Total	16.2	−430.7	−401.4	−159.9	1.4	913.1	93.6	−832.0	−991.9	1008.1
faf-stress										
Northern Hemisphere										
Shallow	−2.62	−13.01	0.54	−17.24	18.30	−9.13	17.92	−12.48	−29.71	27.10
Deep	0.14	−7.12	−7.73	−1.02	14.07	0.00	1.94	−14.84	−15.86	16.01
Total	−2.47	−20.13	−7.19	−18.26	32.37	−9.13	19.85	−27.32	−45.58	43.10
Southern Hemisphere										
Shallow	0.87	−16.53	−0.38	−6.51	1.42	14.84	8.03	−16.91	−23.42	24.29
Deep	1.65	−21.85	13.28	0.93	21.62	−15.54	3.21	−8.57	−7.64	9.29
Total	2.52	−38.38	12.90	−5.58	23.04	−0.69	11.23	−25.48	−31.06	33.58
faf-heat										
Northern Hemisphere										
Shallow	65.73	−19.58	29.76	−7.97	15.44	44.34	3.74	10.18	2.21	63.53
Deep	33.17	18.43	4.70	7.62	3.62	0.28	−1.50	23.14	30.76	2.41
Total	98.90	−1.15	34.47	−0.35	19.07	44.62	2.24	33.32	32.97	65.94
Southern Hemisphere										
Shallow	11.95	10.79	−15.87	5.62	18.78	−4.20	−3.17	−5.09	0.53	11.42
Deep	77.74	43.35	0.15	−7.53	0.52	35.43	5.81	43.50	35.97	41.77
Total	89.70	54.14	−15.72	−1.91	19.31	31.24	2.64	38.42	36.51	53.19

Budget components include the net heat storage (NET), model prognostic advection (ADV), parameterized eddy-induced advection (EDDY), the residual mean advection (rADV), diffusive isopycnal mix (ISO), vertical diffusive processes, super-residual advection (srADV) and vertical diffusive processes, and diapycnal mix plus penetrative heating from shortwave radiation (vDIFF), which includes the interannual unresolved contribution as to close the budgets. Vertical integrals account for the shallow, deep, and total ocean column. Estimations for both hemispheres separately are shown. Results are time-averaged over the last decade of each simulation period. Units are TW $\equiv 10^{12}$ W.

as suggested by the reduced WBC residual transport and the reduced intermediate and deep water masses transport below the cell. In contrast to the NH, wind stress anomalies promote an increase in mid-latitude subduction and poleward transport outside of the cell. The strengthening of the shallow overturning cell and the significantly decreased formation of dense water at higher latitudes is in agreement with observed warming imbalances. In both cases, the shallow and deep oceans warm by increased srADV cooling and vDIFF warming (Figure 8A).

Results in faf-heat are shown in Figure 9. Based on the large surface poleward flow strengthening in mass and heat transports, the NH shallow overturning cell reveals an overall strengthening (approximately 20%) compared to the control run (Figure 9A). This is achieved by the surface layer alone since the WBC is weakened (−6%). In fact, according to the zonally integrated transports (Figure 9B), both poleward surface transport and equatorward upper transport are significantly intensified (20% and ∼ 50%, respectively). Hence, despite a cell circulation strengthening, the net poleward surface transport outside of the cell is weakened, as well as the subsequent downwelling of this water into deeper levels. This is shown by a significant reduction of the residual transport (−35%) and the equatorward intermediate water mass production (−31%).

In contrast, the SH shallow overturning cell reveals a non-significant change in circulation. Once we consider the zonally integrated transport, while the poleward surface transport reveals

TABLE 3 Northern Hemisphere Pacific Ocean meridional mass transport (Sv) and heat transport (PW) across 24°N.

	faf-stress			faf-heat			Control	
	[Sv]	[PW]		[Sv]	[PW]		[Sv]	[PW]
Shallow Overturning Cell								
Surface	13.83	1.27	(2%)	16.31	1.50	(20%)	13.60	1.26
WBC	14.33	1.56	(−20%)	17.06	1.62	(−6%)	18.22	1.64
Interior	−28.16	−2.12	(−11%)	−33.37	−2.72	(5%)	−31.82	−2.34
Residual	5.04	0.34	(8%)	3.06	0.19	(−35%)	4.67	0.32
Imbalance	2.00	0.71		−1.35	0.40	0.47	0.47	0.56
Zonally integrated transport (whole column)								
Surface	13.83	1.27	(2%)	16.31	1.50	(20%)	13.60	1.26
Upper	−8.79	−0.22	(−2%)	−13.25	−0.91	(48%)	−8.93	−0.38
Intermed.	−4.76	−0.34	(0.8%)	−3.26	−0.23	(−31)	−4.72	−0.34
Deep.	−0.52	−0.03	(160%)	0.11	0.02	(45%)	−0.20	0.00
Deep 2	0.24	0.03	(−20%)	0.09	0.02	(−64%)	0.25	0.02
Bottom	0.00	0.00		0.00	0.00		0.00	0.00

Results refer to the annually averaged meridional transports under faf-stress, faf-heat, and the equilibrium-state solution (Control). Our estimations consider mass balance adjusted to zero across 24°N. Meridional transport inside the cell is divided into surface poleward transport, Western Boundary Current transport (WBC), and interior equatorward transport. Balance inside the overturning cell excludes transport within deeper levels of the WBC (Residual), which flows outside of the gyre toward the subpolar region. Both shallow overturning and total heat transport estimations are also shown. The zonally integrated transport for the different density classes, with each water mass classified according to its ventilation level, is also shown. The Upper transport refers to the sum of all fluxes within the shallow overturning cell (poleward WBC plus equatorward interior flow, excluding the surface term). The rest of the terms refer to meridional mass transports below the cell. Relative change of each component with respect to the equilibrium state is shown in brackets. Data are time-averaged over the last decade of each simulation period.

TABLE 4 As in Table 3 but for the Southern Hemisphere meridional mass transport across 24°S.

	faf-stress			faf-heat			Control	
	[Sv]	[PW]		[Sv]	[PW]		[Sv]	[PW]
Shallow Overturning Cell								
Surface	−9.21	−0.97	(9%)	−8.38	−0.88	(−1%)	−8.47	−0.90
WBC	−7.40	−0.74	(−8%)	−8.03	−0.86	(0.1%)	−8.02	−0.83
Interior	16.61	1.71	(0.7%)	16.42	1.74	(−0.4%)	16.49	1.73
Residual	−2.40	−0.24	(−12%)	−1.23	−0.07	(−55%)	−2.72	−0.24
Imbalance	13.49	1.62	(−8%)	13.66	1.61	(−7%)	14.73	1.69
Zonally integrated transport (whole column)								
Surface	−9.21	−0.97	(9%)	−8.38	−0.88	(−1%)	−8.47	−0.90
Upper	6.81	0.73	(18%)	7.16	0.81	(24%)	5.75	0.66
Intermd.	0.04	0.01	(−130%)	−0.11	−0.01	(260%)	−0.03	0.00
Deep	−0.69	−0.06	(−15%)	−0.97	−0.09	(20%)	−0.81	−0.08
Deep 2	3.05	0.21	(−14%)	2.31	0.14	(−35%)	3.56	0.24
Bottom	0.00	0.08		0.00	0.03		0.00	0.08

The Indonesian Throughflow and Bering Strait throughflow (ITF/BS) contributions are also shown. Mass balance in the cell is achieved by subtracting this contribution. The total heat transport estimation includes such contribution, while the shallow overturning term is zero by construction.

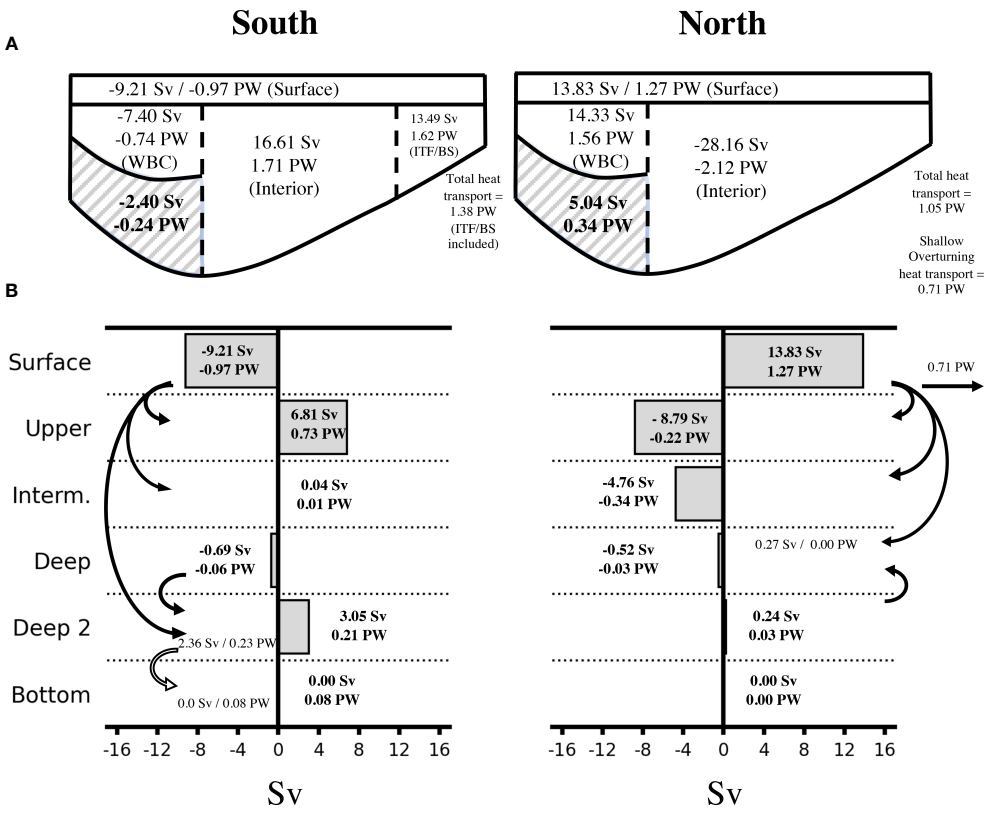

FIGURE 7
As in Figure 4 but for faf-stress.

no significant change, the upper equatorward transport shows a significant increase (25%) compared to the control run. This is explained in terms of the significant reduction of residual transport by the WBC (−55%). This reduction in mass export by the cell towards deeper levels seems to be responsible for the observed deep water production weakening (−35%) and the poleward intermediate-to-deep water strengthening by recirculation of the subducted water. The strengthening of the NH overturning cell, accompanied by the significant weakening of dense water production in both hemispheres (∼ 50%), is in agreement with the shallow and deep ocean net warming (by reduced srADV cooling and increased vDIFF warming). The strengthened cell circulation seems to promote the reduction of the transport of mass and heat out of the cell, thus increasing the retention of warm water by the cell and potentially explaining the increased heat content (Figure 8B). The same intensification of cell circulation seems to promote the reduction of dense water production, thus weakening deep-to-abyssal branches of the overturning circulation (weakened srADV cooling). In the SH, a similar mechanism (reduction of dense water production) may explain the overall warming of the deep ocean. In other words, by reducing dense water production, ventilation of deep ocean is reduced, increasing the retention time for dense water and the heat content as well.

The shallow overturning cell presents significant changes in faf-heat. However, in contrast to faf-stress, where the observed changes are explained in terms of the anomalous wind-driven circulation, in faf-heat, changes in the shallow overturn can be explained in terms of isopycnal dependency of the meridional flow across the cell. The strengthening of the interior pycnocline transport is associated with the intensification of the zonal pycnocline tilt, particularly in the WBC region, due to the coarse-resolution setup (Huber and Zanna, 2017), and by reducing such a strong pycnocline dependency, circulation changes in faf-heat might be significantly reduced. Further analyses are required to assess the impact of the model resolution, parametrizations, and the role of ocean–atmosphere coupled feedbacks.

4 Discussion and conclusions

We have quantified the heat budget and the transport of mass and heat in the tropical Pacific in equilibrium conditions and under surface flux perturbations of heat (faf-heat) and stress (faf-stress) separately. Although not very large, FAFMIP surface anomalies represent the transient response of the climate system to a doubled CO_2 concentrations and are thus suited for investigating possible future ocean dynamical changes (Gregory et al., 2016; Todd et al., 2020). We found that, in the Control state, the shallow tropical Pacific is in equilibrium due to the balance between super residual advection (srADV) cooling and vertical diffusion (vDIFF) warming, both related to the redistribution of water by the shallow overturn,

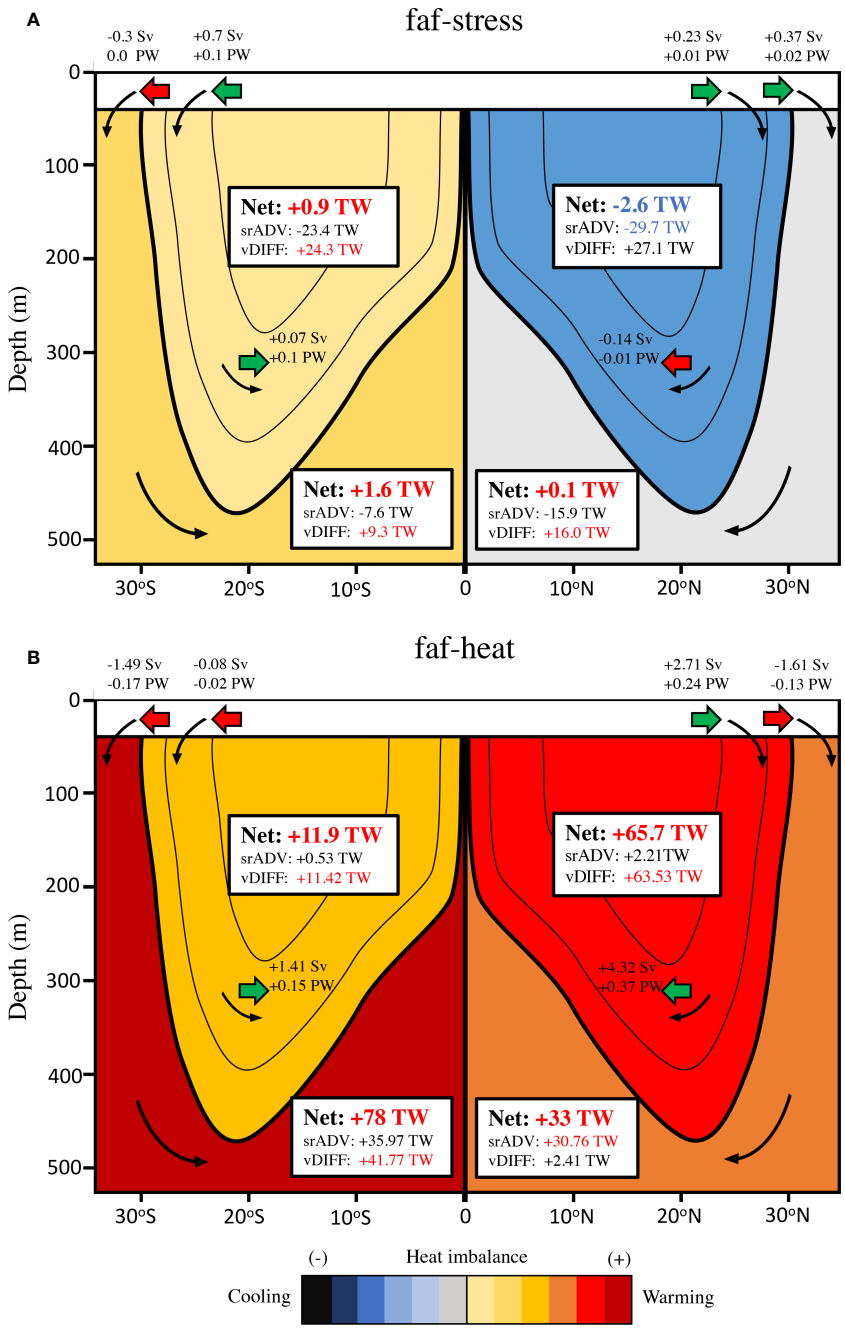

FIGURE 8
Tropical Pacific Ocean circulation and heat budget changes for **(A)** faf-stress and **(B)** faf-heat experiments. The schematics are vertically divided into the mixed layer (top white box), the Shallow Wind-driven Meridional Overturn (black contours), and the deep ocean. Meridional mass transports inside the overturn are represented by horizontal arrows; the direction represents mean conditions and the color either strengthening (green) or weakening (red). The thin black arrows represent the required flow to close the meridional circulation. Meridional mass transport associated with the production of dense water out of the shallow overturn, approximately at 30°S and 30°N, is also shown. Meridional mass and heat transport values are also indicated. Heat budget component anomalies (white boxes), for both shallow and deep oceans, are shown for the super residual advection (srADV), vertical diffusive (vDIFF), and net heat storage term (Net). Heat imbalances within the column are depicted with color shades.

as the cell recirculates most of the surface poleward mass and heat transport. The production of dense water is fully accounted for by the WBC residual transport, as all surface poleward transport subducts in mid-latitudes.

In faf-stress, heat budget imbalances arise as the residual between srADV cooling and vDIFF warming, i.e., a strengthened upwelling–diffusive balance (Figure 8A). Imbalances are triggered by circulation changes promoted by the imposed wind stress perturbation. The NH cell is weakened while dense water production is increased, possibly due to a reduced mid-latitude downwelling of water inside the shallow overturn, given the weakened easterlies and westerlies in the NH. In contrast, the overturning circulation is intensified in SH, while dense water production is weakened. Based on our mass balance analysis, all

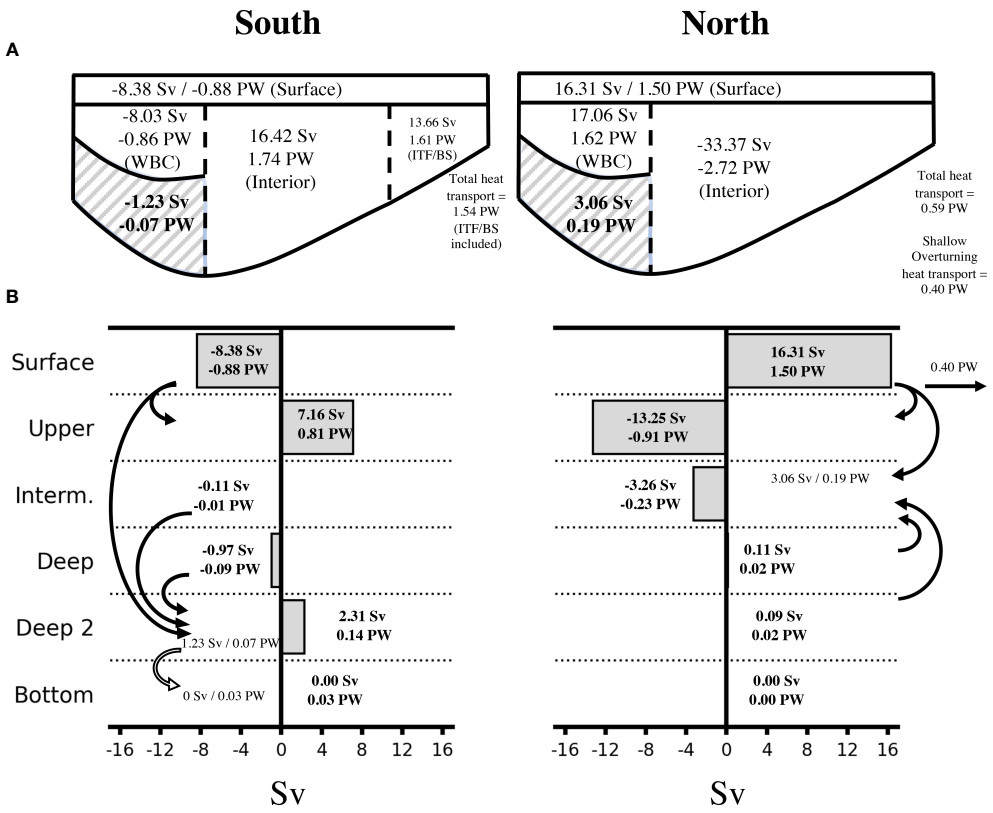

FIGURE 9
As in Figure 4 but for faf-heat.

the strengthened poleward surface water remains inside the gyre, sinking in mid-latitudes and joining the returning flow, while reducing the dense water production at higher latitudes. In line with the positive wind stress perturbation over the region. Additionally, changes in both the heat budget and circulation inside the cell are strongly related. While cooling of the NH shallow overturn matches the weakened circulation, warming of the SH shallow overturns matches the strengthened circulation. In the case of the deep ocean, SH warming is explained in terms of the decreased convergence of dense water.

In faf-heat (Figure 8B), budget imbalances are explained in terms of a reduction of the srADV cooling and an increase in vDIFF warming (weakened upwelling–diffusive balance). The warming of the shallow ocean matches the strengthened circulation of the cell in both hemispheres. Given the lack of a wind-stress perturbation, changes are explained in terms of the isopycnal dependency of the meridional flow. Moreover, changes in the shallow overturning circulation promote changes in the heat content of the cell. The subsequent decrease in dense water production is also explained in similar terms. As in faf-stress, our mass balance analysis suggests a strong relationship between changes in the overturning circulation and in dense water production. Heat budget changes inside the cell oppose the observed changes in dense water production. Hence, changes in the ocean budgets are reflected in the dense water production and shallow overturning circulation changes.

Although differences among experiments exist, in both cases, the surface wind-driven cell is the dominant dynamical feature responsible for the redistribution of mass and heat in the Tropical Pacific, in both shallow and deep ocean.

Finally, acknowledging the limitations in our modeling framework, the analysis presented provides an assessment of the tropical Pacific ocean response under increasing CO_2 concentrations. Our results suggest that most of the changes in heat budget are accounted for by the shallow ocean and mainly promoted by wind-driven cells, although heat anomalous fluxes also have a significant impact on the tropical Pacific circulation. Analysis within coupled models and different climate change scenarios may provide further information on the future evolution of the tropical Pacific Ocean heat budget and circulation.

Data availability statement

The datasets presented in this study can be found in online repositories. The names of the repository/repositories and accession number(s) can be found below: The datasets used in this study can be found at https://doi.org/10.5281/zenodo.7708995 and the FAFMIP forcing fields at https://doi.org/10.5281/zenodo.7709082.

Author contributions

All authors listed have made a substantial, direct, and intellectual contribution to the work and approved it for publication.

Funding

RN-L was supported by an ICTP scholarship to the ESFM PhD Program at the University of Trieste.

Acknowledgments

We thank two reviewers and the associate editor for their excellent suggestions that improved the original manuscript.

Conflict of interest

The authors declare that the research was conducted in the absence of any commercial or financial relationships that could be construed as a potential conflict of interest.

Publisher's note

References

Banks, H., and Gregory, J. (2006). Mechanisms of ocean heat uptake in a coupled climate model and the implications for tracer based predictions of ocean heat uptake. *Geophys. Res. Lett.* 33, L07608. doi: 10.1029/2005GL025352

Dias, F., Domingues, C., Marsland, S., Griffies, S., Rintoul, S., Matear, R., et al. (2020). On the superposition of mean advective and eddy-induced transports in global ocean heat and salt budgets. *J. Clim.* 33, 1121–1140. doi: 10.1175/JCLI-D-19-0418.1

England, M. H., McGregor, S., Spence, P., Meehl, G. A., Timmermann, A., Cai, W., et al. (2014). Recent intensification of wind-driven circulation in the Pacific and the ongoing warming hiatus. *Nat. Geosci.* 4, 222–227. doi: 10.1038/nclimate2106

Exarchou, E., Kuhlbrodt, T., Gregory, J., and Smith, R. (2014). Ocean heat uptake processes: A model intercomparison. *J. Clim.* 28, 887–908. doi: 10.1175/JCLI-D-14-00235.1

Farneti, R., Molteni, F., and Kucharski, F. (2014). Pacific interdecadal variability driven by tropical extratropical interactions. *Clim. Dyn.* 42, 3337–3355. doi: 10.1007/s00382-013-1906-6

Fox-Kemper, B., Danabasoglu, G., Ferrari, R., Griffies, S., Hallberg, R., Holland, M., et al. (2011). Parameterization of mixed layer eddies. iii: Implementation and impact in global ocean climate simulations. *Ocean Model.* 39, 61–78. doi: 10.1016/j.ocemod.2010.09.002

Fox-Kemper, B., Ferrari, R., and Hallberg, R. (2008). Parameterization of mixed layer eddies. part i: Theory and diagnosis. *J. Phys. Oceanogr.* 38, 1145–1165. doi: 10.1175/2007JPO3792.1

Garuba, O., and Klinger, B. (2016). Ocean heat uptake and interbasin transport of passive and redistributive surface heating. *J. Clim.* 29, 7507–7527. doi: 10.1175/JCLI-D-16-0138.1

Gastineau, G., Friedman, A. R., Khodri, M., and Vialard, J. (2019). Global ocean heat content redistribution during the 1998–2012 interdecadal pacific oscillation negative phase. *Clim. Dyn.* 53, 1187–1208. doi: 10.1007/s00382-018-4387-9

Gent, P., and McWilliams, J. C. (1990). Isopycnal mixing in ocean circulation models. *J. Phys. Oceanogr.* 20, 150–155. doi: 10.1175/1520-0485(1990)020<0150:IMIOCM>2.0.CO;2

Gent, P. R., Willebrand, J., McDougall, T. J., and McWilliams, J. C. (1995). Parameterizing eddy-induced tracer transports in ocean circulation models. *J. Phys. Oceanogr.* 25, 463–474. doi: 10.1175/1520-0485(1995)025<0463:PEITTI>12.0.CO;2

Graffino, G., Farneti, R., Kucharski, F., and Molteni, F. (2018). The effect of wind stress anomalies and location in driving pacific subtropical cells and tropical climate. *J. Clim.* 32, 1641–1660. doi: 10.1175/JCLI-D-18-0071.1

Graffino, G., Farneti, R., Kucharski, F., and Molteni, F. (2019). The effect of wind stress anomalies and their location in driving Pacific Subtropical cells and tropical climate. *J. Clim.* 32, 1641–1660. doi: 10.1175/JCLI-D-18-0071.1

Gregory, J. M. (2000). Vertical heat transports in the ocean and their effect on time-dependent climate change. *Clim. Dyn.* 16, 501–515. doi: 10.1007/s003820000059

Gregory, J. M., Bouttes, N., Griffies, S. M., Haak, H., Hurlin, W. J., Jungclaus, J., et al. (2016). The flux-anomaly-forced model intercomparison project (fafmip) contribution to cmip6: investigation of sea-level and ocean climate change in response to co2 forcing. *Geosci. Model. Dev.* 9, 3993–4017. doi: 10.5194/gmd-9-3993-2016

Griffies, S. M. (1998). The gent–mcWilliams skew flux. *J. Phys. Oceanogr.* 28, 831–841. doi: 10.1175/1520-0485(1998)028<0831:TGMSF>2.0.CO;2

Griffies, S. (2012). Elements of the modular ocean model (mom): 2012 release. *Elements Modular Ocean Model. (MOM)* (NOAA/Geophysical Fluid Dynamics Laboratory), 7.

Griffies, S. M., Danabasoglu, G., Durack, P. J., Adcroft, A. J., Balaji, V., Boning, C. W., et al. (2016). Omip contribution to cmip6: experimental and diagnostic protocol for the physical component of the ocean model intercomparison project. *Geosci. Model. Dev.* 9, 3231–3296. doi: 10.5194/gmd-9-3231-2016

Huber, M. B., and Zanna, L. (2017). Drivers of uncertainty in simulated ocean circulation and heat uptake. *Geophys. Res. Lett.* 44, 1402–1413. doi: 10.1002/2016GL071587

Klinger, B., and Marotzke, J. (2000). Meridional heat transport by the subtropical cell. *J. Phys. Oceanogr.* 30, 696–705. doi: 10.1175/1520-0485(2000)030<0696:MHTBTS>2.0.CO;2

Kuhlbrodt, T., Gregory, J., and Shaffrey, L. (2015). A process-based analysis of ocean heat uptake in an aogcm with an eddy-permitting ocean component. *Clim. Dyn.* 45, 3205–3226. doi: 10.1007/s00382-015-2534-0

Large, W. G., McWilliams, J. C., and Doney, S. C. (1994). Oceanic vertical mixing: A review and a model with a nonlocal boundary layer parameterization. *Rev. Geophys.* 32, 363–403. doi: 10.1029/94RG01872

Levitus, S. (1982). *Climatological atlas of the world ocean* (Princeton, N.J.: NOAA/ERL GFDL Professional Paper 13), 173.

Marshall, J., Scott, J., Armour, K., Campin, J.-M., Kelley, M., and Romanou, A. (2014). The ocean's role in the transient response of climate to abrupt greenhouse gas forcing. *Clim. Dyn.* 44, 2287–2299. doi: 10.1007/s00382-014-2308-0

McCreary, J., and Lu, P. (1994). Interaction between the subtropical and equatorial ocean circulations— the subtropical cell. *J. Phys. Oceanogr.* 24, 466–497. doi: 10.1175/1520-0485(1994)024<0466:IBTSAE>2.0.CO;2

McPhaden, M., and Zhang, D. (2002). Slowdown of the meridional overturning circulation in the upper pacific ocean. *Nature* 415, 603–608. doi: 10.1038/415603a

McPhaden, M., and Zhang, D. (2004). Pacific ocean circulation rebounds. *Geophys. Res. Lett.* 31, L18301. doi: 10.1029/2004GL020727

Song, L., Li, Y., Wang, J., Hu, S., Liu, C., Diao, X., et al. (2018). Tropical meridional overturning circulation observed by subsurface moorings in the western pacific. *Sci. Rep.* 8, 2045–2322. doi: 10.1038/s41598-018-26047-7

Talley, L. (2003). Shallow, intermediate, and deep overturning components of the global heat budget. *J. Phys. Oceanogr.* 33, 530–560. doi: 10.1175/1520-0485(2003)033<0530:SIADOC>2.0.505CO;2

Taylor, K., Ronald, S., and Meehl, G. (2011). An overview of cmip5 and the experiment design. *Bull. Am. Meteorol. Soc.* 93, 485–498. doi: 10.1175/BAMS-D-11-00094.1

Todd, A., Zanna, L., Couldrey, M., Gregory, J., Wu, Q., Church, J. A., et al. (2020). Ocean-only fafmip: Understanding regional patterns of ocean heat content and dynamic sea level change. *J. Adv. Model. Earth Syst.* 12, e2019MS002027. doi: 10.1029/2019MS002027

Xie, P., and Vallis, G. (2011). The passive and active nature of ocean heat uptake in idealized climate change experiments. *Clim. Dyn.* 38, 667–684. doi: 10.1007/s00382-011-1063-8

Zhang, D., and McPhaden, M. (2006). Decadal variability of the shallow pacific meridional overturning circulation: Relation to tropical sea surface temperatures in observations and climate change models. *Ocean Model.* 15, 250–273. doi: 10.1016/j.ocemod.2005.12.005